Action Potential Characteristics and Arrhythmogenic Properties of the Cardiac Conduction System of the Murine Heart

Justus M.B. Anumonwo, Yvonne N. Tallini, Frederick J. Vetter, José Jalife

Abstract—Studies have characterized conduction velocity in the right and left bundle branches (RBB, LBB) of normal and genetically engineered mice. However, no information is available on the action potential characteristics of the specialized conduction system (SCS). We have used microelectrode techniques to characterize action potential properties of the murine SCS, as well as epicardial and endocardial muscle preparations for comparison. In the RBB, action potential duration at 50%, 70%, and 90% repolarization ($APD_{50,70,90}$) was 6 ± 0.7, 35 ± 6, and 90 ± 7 ms, respectively. Maximum upstroke velocity (dV/dt_{max}) was 153 ± 14 V/s, and conduction velocity averaged 0.85 ± 0.2 m/s. APD_{90} was longer in the Purkinje network of fibers (web) than in the RBB ($P<0.01$). Web APD_{50} was longer in the left than in the right ventricle ($P<0.05$). Yet, web APD_{90} was longer in the right than in the left ventricle ($P<0.001$). $APD_{50,70}$ was significantly longer in the endocardial than in the epicardial ($P<0.001$; $P<0.003$). APD_{90} in the epicardial and endocardial was shorter than in the RBB (≈36 ms versus ≈100 ms). Spontaneous electrical oscillations in phase 2 of the SCS occasionally resulted in early afterdepolarizations. These results demonstrate that APDs in the murine SCS are significantly (≈2-fold) longer than in the myocardium and implicate the role of the murine SCS in arrhythmias. The differences should have important implications in the use of the mouse heart to study excitation, propagation, and arrhythmias. (*Circ Res*. 2001;89:329-335.)

Key Words: action potential ■ His bundle ■ Purkinje ■ right bundle ■ myocyte

With the development of genetically engineered mouse technology, and the possibility to study the roles of specific ion channel proteins in the cardiac excitation, the murine experimental model has become a valuable tool in the investigation of the cardiac excitation process.[1–6] However, the ionic mechanism underlying excitation of the heart in any species is dependent on the specific set of ion channel proteins expressed in the particular type of heart tissue, and an adequate use of a genetically altered heart requires, as an important first step, a sufficient understanding of its basic cardiac electrophysiology.

There are reports in the literature on action potential characteristics and ionic current mechanisms in cells from the murine working myocardium.[7–12] In comparison, little information is available on the specialized conduction system of the mouse heart. Histological evidence, however, suggests that the fibers are distributed in a similar manner to that seen for larger animals and in humans.[13–15] In such hearts, for example, the atrioventricular node gives rise to a compact right bundle branch (RBB) that inserts into the intraventricular septum, with or without branching. In canines and humans, there is evidence that the left bundle branch (LBB), in contrast to the RBB, gives off several branches as it inserts into the septum and the ventricular free wall. Electrophysiological reports from such species show that, characteristi-

cally, Purkinje cells of the specialized conduction fibers have relatively negative resting potentials, a high rate of upstroke velocity, long action potential duration (APD) and a low internal resistance. Additionally, the cells demonstrate automaticity, which, however, is normally suppressed by the spontaneous activity of the dominant pacemaker cells of the sinus node.[16–18]

Atrioventricular propagation was recently studied in wild-type and mutant mice,[19,20] and it was reported that targeted disruption of the gap junction protein connexin40 (Cx40) led to conduction abnormalities. Cx40 is the gap junction channel protein predominantly expressed in the His-Purkinje system. Recently, using a high-resolution optical mapping technique, we demonstrated slow propagation in the RBB of Cx40 knockout mice.[5] To our knowledge, however, there is no report in the literature on the action potential characteristics of the murine specialized conduction system. Furthermore, it is unknown whether abnormal spontaneous activity occurs in these cells as has been demonstrated for other species. The adult mouse averages 5 to 7 mm from base to apex and the left ventricular transmural dimensions are proportionately small. The left ventricular free wall, for example, is ≈750 μm thick.[21] The diameter of the specialized conduction system fibers in the Purkinje network measures in the tens of microns at the most. The small size of the fibers clearly imposes

technical constraints with regard to cell isolation. Optical mapping techniques are invaluable for propagation studies because they allow for multiple site recordings on the cardiac surface. In our previous study of propagation in the murine specialized conduction system, we showed that the RBB optical upstrokes precede the QRS complexes only by ≈3 ms. Thus, muscle activation effectively masks the optical signal of repolarization in the RBB. In this investigation, we have used the conventional microelectrode technique to profile the basic electrophysiology of cells in the murine specialized conduction fibers.

Materials and Methods

Experiments were carried out in septal tissue preparations (wedges) of mouse (Swiss Webster; Taconic, Germantown, NY) hearts, which contained Purkinje fibers in a web, as well as the RBB. Animals were cared for in accordance with guidelines described in the *Guide for the Care and Use of Laboratory Animals*, prepared by the Institute of Laboratory Animal Resources National Research Council. After isolation of the heart, the atria were removed from along the atrioventricular ring. Very carefully, the left and right ventricular free walls were then removed. The remaining wedge of septal tissue containing the Purkinje fibers could then be pinned down flat on either side and superfused. For the epicardial recordings, microelectrode impalements were made on the free wall of the right ventricle. The endocardial recordings were obtained from the septum. All recordings were performed in normal Tyrode solution,[5,22] using the standard microelectrode technique (DC resistance of 20 to 30 MΩ when filled with 3 mol/L KCl) on the stage of an Olympus SZ40 microscope, at 38±1°C. The preparations were driven using bipolar stimulating microelectrodes at pulse amplitudes of 0.2 to 0.3 mA, pulse duration of 2 ms, and basic cycle length (BCL) of 300 ms, except where otherwise stated. To pace the RBB, the stimulating electrodes were placed proximally, at the base end of the wedge preparation. Conduction velocity was measured by simultaneous impalements of fibers on the RBB. Staining of the conduction fibers was carried out as previously described,[5] using the acetylthiocholine iodide (ATCHI) stain.[23] All data acquisition and analyses were carried out using pClamp (version 6) suite of programs (Axon Instruments), which was installed on a microcomputer. Data are presented as mean±SEM. When appropriate, statistical analyses were performed using ANOVA, and differences between subgroups were determined using the Bonferroni correction. Differences were considered significant at a value of $P<0.05$.

Results

Morphology and Action Potential Properties of the Mouse His-Purkinje

In a previous report,[5] we used high-resolution optical maps to study impulse propagation in the RBB of the right ventricular septal wall of the mouse. In that study, the path of impulse propagation correlated well with a segment of the RBB, as revealed by the ATCHI stain. ATCHI precipitates in the presence of acetylcholinesterase activity that is present on the Purkinje cells of the conduction system.[5,23] In the present study, we used a combination of ATCHI stain and microelectrode impalements to characterize the electrophysiology of the mouse conduction system.

Figure 1 is a set of photomicrographs of the right ventricular septal wall. In Figure 1A, the right ventricular free wall has been resected to show the structures in the ventricular cavity. Figure 1B is a close-up of the boxed area in Figure 1A and shows the extensive network of Purkinje fibers (referred to hereafter as the web) within the cavity. The shadow of a
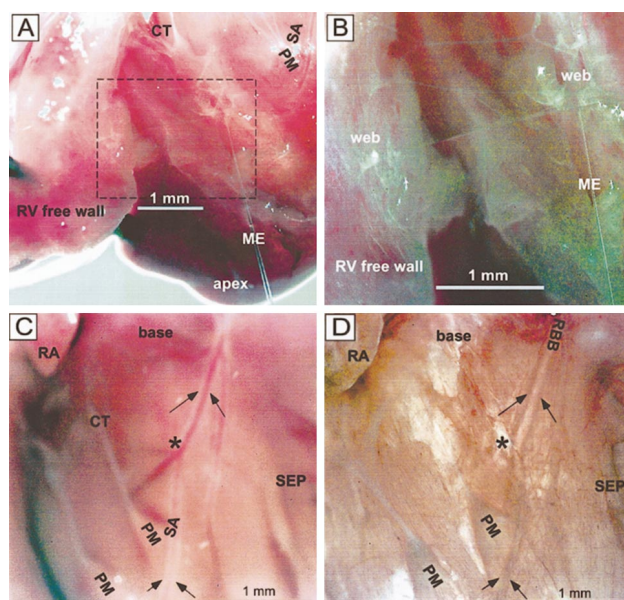

Figure 1. Distribution of the cardiac conduction system in the right ventricle of the mouse heart. A, Low-power view of right ventricular cavity showing the main features of the wedge preparation. B, Section of panel A shown in a higher magnification. Note the extensive network of Purkinje fibers and the shadow of a microelectrode. C, Photomicrograph of another septal preparation showing the septal wall with associated septal artery, the papillary muscle, and the chordae tendineae of the tricuspid valve. D, Preparation shown in panel C after staining with ATCHI. ME indicates microelectrode; CT, chordae tendineae; SA, septal artery; PM, papillary muscle; RV, right ventricle; RA, right atrium; SEP, septum; and RBB, right bundle branch.

microelectrode can be seen in both Figures 1A and 1B. Figure 1C was taken from another heart and shows the septal wall with the associated septal artery, the papillary muscle as well as the chordae tendineae of the tricuspid valve. Another image of this heart is shown in Figure 1D after staining with ATCHI. In this heart, the fibers of the RBB and its branches could be visualized as brown structures (arrows) running alongside the septal wall artery. As shown in Figure 1D, staining of fibers left an imprint or a shadow of the blood vessel. Note that in the preparation the septal artery is forked at the proximal (base) end as well as at about halfway toward the apex (indicated by the asterisk), as it runs toward the anterior papillary muscle. Importantly, note that the branch of the septal artery is devoid of the fibers. Consistent with this is the lack of staining along the edges of this vessel in Figure 1D (asterisks). During the isolation of the preparation, inspection of the septal wall and the endocardial surfaces of the right and left showed several Purkinje fiber branches, which in several cases, visibly, were spontaneously active. This conspicuous distribution of the fibers, especially along the septal artery, facilitated the microelectrode recordings in this study.

Consistent with the ATCHI stain of the fibers of the conduction system (shown in Figure 1), a microelectrode map of the right ventricular septal wall revealed a distinct profile of the action potentials, which could be recorded from cells along the septal artery, indicating that the RBB (or a branch of it) runs parallel to an artery that is midline on the septal wall to approximately two-thirds down the septum. To
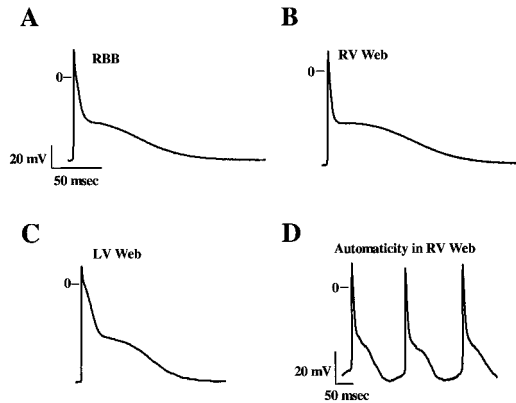
Figure 2. Properties of action potentials recorded from the mouse cardiac conduction system. A, Action potential recording from the RBB. B, Action potential recorded from the right ventricular web. C, Action potential recording from the left ventricular web. D, Spontaneous activity recorded from a fiber in the right ventricular web preparation. Calibration in panel A is also applicable to panels B and C.

characterize regional action potential profiles of the specialized conduction system (Figure 2), electrical recordings (BCL=300 ms) were carried out from the RBB (Figure 2A) as well as from the web in the right (Figure 2B) and left (Figure 2C) ventricles. The action potentials were characterized by a prominent phase 1 repolarization and a very distinct phase 2, which occurred usually between −15 and −50 mV. In a few cases, especially from cells within the web, phase 1 repolarization was followed by a transient depolarization resulting in a characteristic notch or a spike-and-dome configuration reported for some cardiac cells.[24–26] This action potential property is discussed in a later section. Figure 2D shows spontaneous action potentials recorded from a fiber within the web of the right ventricle.

TABLE 1. Comparison of Action Potential Parameters in the Mouse Conduction Fibers

Parameter	Right Bundle Branch (N=6; n=8)	Right Ventricular Web (N=6; n=9)	Left Ventricular Web (N=6; n=8)
RMP, mV	−77±3	−80±1	−75±2
APA, mV	84±5	97±1	89±4
APD_{50}, ms	6±0.7*†	10±2‡	13±1
APD_{70}, ms	35±6§	55±3‖	33±4
APD_{90}, ms	90±7¶#	101±5**	67±4
dV/dt_{max}, V/s	153±14	217±26	154±12
CV, m/s	0.85±0.2	ND	ND

Values are mean±SEM (N indicates number of animals; n, number of fibers). RMP indicates resting membrane potential; APA, action potential amplitude; $APD_{50,70,90}$, action potential duration, respectively, at 50%, 70%, and 90% repolarization; dV/dt_{max}, maximum rate of depolarization at upstroke; and ND, not determined. Preparations were stimulated at 300 BCL.

*$P<0.01$ vs right ventricular (RV) web.
†$P<0.001$ vs left ventricular (LV) web.
‡$P<0.05$ vs LV web.
§$P<0.001$ vs RV web.
‖$P<0.01$ vs LV web.
¶$P<0.01$ vs RV web.
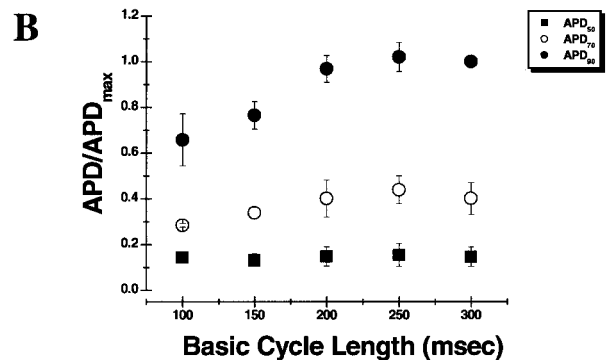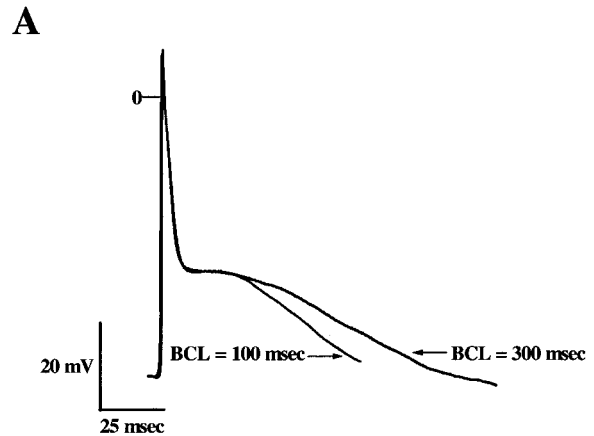#$P<0.001$ vs LV web.
**$P<0.001$ vs LV web.

Figure 3. Effect of stimulus BCL on APD in the mouse RBB. A, Superimposition of two action potentials in an RBB fiber at BCL of 100 and 300 ms. B, Plot of APD as a function of BCL, normalized to duration at BCL of 300 ms.

Action potential parameters from the RBB and the webs of the right and left ventricles are presented in Table 1. These results show that the action potential duration of cells in the mouse conduction fibers is very long (APD at 90% repolarization [APD_{90}] is ≈90 ms in the RBB) and has a very distinct profile of a prominent phase 2. The data in Table 1 show that His-Purkinje fiber maximum APDs were significantly longer in the right ventricle compared with the left ventricle. However, in the webs, APD_{50} was significantly longer in the left than in the right ventricles ($P<0.05$). Yet web APD_{90} was larger in the right than in the left ventricle. In a separate set of experiments, we determined the effect of the pacing rate (BCL=100 to 300 ms) on the action potential properties of the RBB (Figure 3). In Figure 3A, action potentials recorded at 100-ms and 300-ms BCL have been superimposed. The action potential at a BCL of 100 ms was truncated to eliminate stimulus artifact. Results from three cells are summarized in Figure 3B, and the results show that compared with a BCL of 300 ms, APD_{90} was significantly reduced at a BCL of 100 ms. Note also that APD_{50} was unchanged by the different pacing rates.

We have compared in Figure 4 the properties of action potentials recorded from cells in the epicardial (Figure 4A) and endocardial (septal, Figure 4B) surfaces of the right
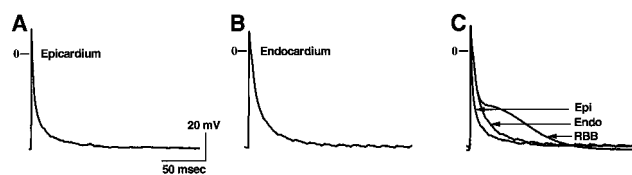
Figure 4. Comparison of the morphologies of action potentials recorded in the murine epicardial (A) and endocardial (B) preparations. In panel C, the action potentials shown panels A and B have been superimposed with an action potential from the RBB. Superimposition was done using the zero voltage level. Epi indicates epicardium; Endo, endocardium; and RBB, right bundle branch. Calibration bars in panel A are applicable to all panels.

ventricular working myocardium. Recordings were carried out on the septum to compare APDs between the cells in the RBB and in the adjacent muscle. Figure 4C is a superimposition of an epicardial, an endocardial, and an RBB recording. The action potential parameters for the epicardial and endocardial preparations have been presented in Table 2 for comparison. The action potential duration was significantly longer in the specialized conduction fibers than in the myocardium. Importantly, these durations are longer than any previously reported values from cells isolated from the murine myocardium. At the pacing rates in these experiments (BCL=300 ms), the action potentials were ≈2 to 3 times longer than the values reported for myocardial cells. Several reports have shown that there are regional differences in APD in the myocardium of several species.[27–31] In one of these studies, it was shown that, in the mouse, APDs were significantly longer in cells isolated from the septum than in those from the apex.[30] In addition, it was reported that APD_{75} is nearly 50% longer at the base compared with the apex.[31] An examination of Table 2 shows that our results are consistent with such findings, given that $APD_{50,70}$ in the endocardium was significantly longer than in the epicardium.

As stated previously, a microelectrode map of the septal wall revealed the approximate path of the RBB on the septal wall. Using multiple electrode impalements during bipolar stimulation, we estimated the speed of impulse propagation along the conduction fibers. The stimulating electrode was placed at the base of the septal preparation, and the micro-

TABLE 2. Comparison of Action Potential Parameters in the Mouse Epicardium and Endocardium

Parameter	Epicardium (N=5; n=12)	Endocardium (N=5; n=7)
RMP, mV	−73±1	−77±.7
APA, mV	77±2	94±2
APD_{50}, ms	3±0.3	8±0.4*
APD_{70}, ms	10±1	15±0.7†
APD_{90}, ms	36±3	37±3
dV/dt_{max}, V/s	114±12	154±10

Values are mean±SEM (N indicates number of animals; n, number of cells). RMP indicates resting membrane potential; APA, action potential amplitude; $APD_{50,70,90}$, action potential duration, respectively, at 50%, 70%, and 90% repolarization; and dV/dt_{max}, maximum rate of depolarization at upstroke. Preparations were stimulated at 300 BCL.

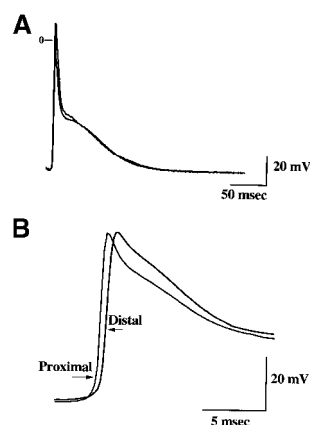*$P<0.001$, †$P<0.003$ vs epicardium.

Figure 5. Measurement of conduction velocity in the mouse RBB using simultaneous impalements. A, Two action potentials (proximal and distal to stimulating electrode) recorded in a fiber bundle along the septal artery (zero voltage refers to proximal action potential). B, Expansion of the time base in panel A illustrating delay of propagation between the proximal and the distal recording electrodes, which were 1.2 mm apart.

electrode impalements for recording were made distal to the stimulating electrode, toward the apex of the heart. These measurements were carried out in three septal preparations, an example of which is shown in Figure 5. The figure shows two His-Purkinje action potentials recorded along a fiber, with simultaneous impalements of two microelectrodes placed 1.2 mm apart. Note the characteristic profile of the His-Purkinje action potential as shown in Figure 2. Figure 5B is an expansion of the time base illustrating the delay in propagation to the proximal and distal recording electrodes. In this preparation, conduction velocity was 1.1 m/s, and in three different preparations averaged 0.85±0.2 m/s (Table 1). Using a high-resolution optical mapping technique, we had previously reported propagation velocity of 0.75 m/s in the RBB of the mouse.[5]

Early Afterdepolarizations in the Mouse His-Purkinje System

As previously stated, in cells within the network of fibers in the endocardial surface, phase 1 repolarization is occasionally followed by a transient depolarization resulting in a characteristic spike-and-dome configuration (Figure 6A). However, note the relatively negative value of potential at which this depolarization occurs. In some instances, cells with the morphology demonstrated spontaneous electrical oscillations in phase 2, which occasionally resulted in early afterdepolarizations (EADs). In this study, we could record EADs in 3 of the 10 preparations investigated. Properties of EADs in one of these preparations are shown in Figures 6B and 6C. After impalement, the BCL was increased from 300 to 400 ms. Figure 6B is a 7-second recording period from the same fiber showing seven normal action potentials and two incidents of EADs (BCL=400 ms). In the same cell, when the BCL was increased to 500 ms (Figure 6C), all responses to the stimulus resulted in EADs.

Discussion

We have characterized the action potential morphology and arrhythmogenic properties of cells in the murine specialized
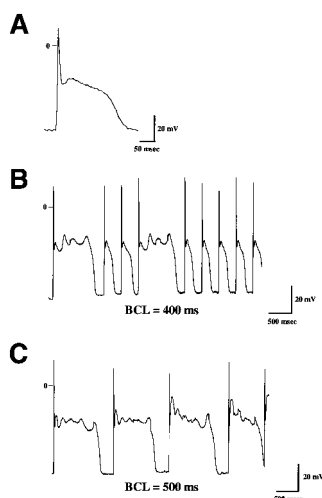
Figure 6. Recordings of EADs in a fiber of the mouse cardiac conduction system. A, Action potential recorded from the right ventricular web preparation showing a prominent spike-and-dome configuration. Calibration bars are 20 mV and 50 ms. B, Recording from the same fiber showing seven normal action potentials and two incidents of EADs after the BCL was changed from 300 to 400 ms. C, Records from the same fiber as in panels A and B, with the BCL increased to 500 ms. Recording durations were $\approx$7 seconds in panels B and C. In panels B and C, calibration bars are 20 mV and 500 ms.

conduction system. The action potential has a very long duration, with a characteristic profile (prominent phase 2) not previously reported for cells isolated from the murine myocardium. This profile was observed for cells in the Purkinje cell network (web) of the right and left ventricles, as well as in the RBB fibers on the septal wall. Stimulating at shorter BCLs reduced the APD_{90} but not the APD_{50}. Action potential configuration from the neighboring (septal) endocardium as well as the epicardium had very different action profiles. In comparison with the data reported for other species, the mouse His-Purkinje action potentials are significantly much longer than those recorded from the epicardial or endocardial ventricular myocardium. The data also indicate a potential role of the specialized conduction system in arrhythmogenesis in the mouse heart.

Electrophysiology of the Murine Specialized Conduction System

The combination of the ATCHI stain and microelectrode impalements has shown that the distribution of the RBB and Purkinje fibers of the mouse conduction system is, in general, similar to that reported in other species.[14,15] However, in the mouse strain investigated (Swiss Webster), we found that the RBB was, very frequently, intimately associated with the septal artery in the right ventricle and could be visualized under bright field as white fibers running along the artery in base to apex direction. Our investigation provides the first available data on the action potential properties of the murine His-Purkinje system.

Several of the electrophysiological characteristics presented in this study are consistent with data from Purkinje cells from other species.[15,32] In one of these studies, action potential properties of Purkinje cells were profiled in cow, sheep,

and canine.[32] The freshly isolated cells had a maximum diastolic potential of -70 and -85 mV, upstroke velocity of 150 to 750 V/s, and an overshoot of about $+30$ mV. Those results also showed that cells rapidly repolarized to a plateau phase between -15 and -30 mV. The Purkinje cell properties are thought to provide adequate propagation as well as ensure safe mechanism against reentrant circuits during cardiac excitation.[15] In comparison with other species,[32] however, our results in the mouse show that at BCLs of 300 ms, APDs are much longer (2- to 3-fold; $\approx$100 ms versus 36 ms) in the murine His-Purkinje, than in the muscle cell. It must nevertheless be stated that, in comparison to these other species, the murine APD is relatively very short. Also, our results show that His-Purkinje fiber APD_{90} is longer in the right ventricle compared with the left ventricle, as has been previously reported for the canine specialized conduction system.[15] In the mouse, the heart rate is $\approx$200 to 636 bpm[19,22,33,34]; a rhythm with cycle length of 100 ms is therefore conceivable. Our results also show that at a BCL of 100 ms, the His-Purkinje action potentials are still significantly (2-fold) longer than in the muscle. The APD_{50} was unchanged by faster (BCL=100 ms) pacing, and the action potentials retained a prominent phase 2.

Characteristically, cells isolated from the murine myocardium have brief action potential durations, with ADP_{90} averaging $\approx$25 to 40 ms.[9–11,30] In the myocardial cells, a prominent role in membrane repolarization has been ascribed to four kinetically distinct K^+ currents.[35] The myocytes had a rapidly inactivating transient outward current ($I_{to,f}$), a slowly inactivating current ($I_{K,slow}$), a noninactivating, steady-state current (I_{ss}), and, in a small subset of the cells that lacked $I_{to,f}$, a slowly inactivating transient outward current dubbed $I_{to,s}$. In another study,[30] the investigators reported that action potential waveforms were distinct in the murine septum and apex, which they attributed to differences in the expression of the fast and slow components of the transient outward current. For example, it was reported that whereas $I_{to,f}$ was present in all left ventricular apex cells and most of the cells isolated from the septum, $I_{to,s}$ was exclusively confined to cells from the left ventricular septum. Importantly, it was shown that APD_{70} was twice as long in the septum than in the apex. Although we have not carried out any measurements of ionic currents in the His-Purkinje cells in the present study, we speculate that qualitative and quantitative differences in expression of the identified ion channels underlie the His-Purkinje cell action potential waveform.

EADs in the Mouse Conduction System

Our results also showed that the action potential waveform of cells in the network branches of the RBB (spike and dome profile) occasionally resulted in EADs. Afterdepolarizations are spontaneous oscillations in membrane potential that occur during and after the repolarization process and are thought to involve abnormalities in the ionic current mechanisms associated with repolarization.[36] It has been suggested that, potentially, these oscillations may be arrhythmogenic by forming impulses repetitively in the myocardium.[36,37] A hallmark feature of the afterdepolarizations is their frequency dependence. The incidence of an EAD is increased as the

BCL is increased, with the opposite effect seen with delayed afterdepolarizations (DADs[37]).

Previous experimental and simulation studies have shown that EADs are increased with low-frequency pacing.[38,39] The studies show that the L-type calcium current is necessary as a depolarizing charge carrier during the EAD. It was also demonstrated that the relative contributions of the calcium current (I_{Ca}) and the delayed rectifier current (I_K) to the total membrane current (in the period critical for EAD formation) determined the incidence of the EAD. At relatively slow rates, there is a net inward current, favoring EAD formation. However, the activation/deactivation properties of I_K at relatively fast rates of pacing allow a significant amount of I_K to remain, enough to offset the inward current, and to prevent the formation of EADs.[38] The molecular mechanism of EAD formation in the Purkinje cells of the murine specialized conduction system cells, however, will be unknown until the nature of the ionic currents in the cells is characterized.

We did not record any EADs or DADs in the murine muscle tissue preparations. This is consistent with data from a relatively recent study showing that no EADs could be recorded in isolated murine wild-type cells with pacing at 1 or 3 Hz.[40] However, it was reported that EADs could be recorded from the myocardium of a mutant (Kv4.2W362F× Kv1.4[−/−]) mouse.[40] Interestingly, the EADs showed a frequency dependence of the type seen for DADs. The presence of EADs in the specialized conduction system may be attributable to the comparatively long duration of repolarization in the Purkinje fiber. It is expected that the relatively negative values of membrane potential in phase 2 will enable the reactivation of depolarizing ionic currents and will predispose the fibers to these oscillations. It is also expected that the negative voltage of the plateau may indicate different ionic mechanisms for the EADs in the mouse than in most other species. It is noteworthy, though, that similarly negative membrane potential value for phase 2 was shown for Purkinje cells isolated from the sheep.[32]

In conclusion, we have profiled, for the first time, the electrophysiology of the murine specialized conduction system. The action potential characteristics shown in the present study have not been previously reported for cells isolated from anywhere in the murine myocardium. The data indicate a potential role of the specialized conduction system in arrhythmogenesis in the mouse heart. In general, the data are important for understanding the excitation process as well as future modeling studies on the murine myocardium.

Acknowledgments

References

1. Babinet C, Morello D, Renard JP. Transgenic mice. *Genome*. 1989;31: 938–949.
2. James JF, Hewett TE, Robbins J. Cardiac physiology in transgenic mice. *Circ Res*. 1998;82:407–415.
3. London B, Wang DW, Hill JA, Bennett PB. The transient outward current in mice lacking the potassium channel gene Kv1.4. *J Physiol*. 1998;509(pt 1):171–182.
4. Kirchhoff S, Kim JS, Hagendorff A, Thonnissen E, Kruger O, Lamers WH, Willecke K. Abnormal cardiac conduction and morphogenesis in connexin40 and connexin43 double-deficient mice. *Circ Res*. 2000;87: 399–405.
5. Tamaddon HS, Vaidya D, Simon AM, Paul DL, Jalife J, Morley GE. High-resolution optical mapping of the right bundle branch in connexin40 knockout mice reveals slow conduction in the specialized conduction system. *Circ Res*. 2000;87:929–936.
6. Saffitz JE, Schuessler RB. Connexin40, bundle-branch block, and propagation at the Purkinje-myocyte junction. *Circ Res*. 2000;87:835–836.
7. Nuss HB, Marban E. Electrophysiological properties of neonatal mouse cardiac myocytes in primary culture. *J Physiol*. 1994;479(pt 2):265–279.
8. Davies MP, An RH, Doevendans P, Kubalak S, Chien KR, Kass RS. Developmental changes in ionic channel activity in the embryonic murine heart. *Circ Res*. 1996;78:15–25.
9. Barry DM, Xu H, Schuessler RB, Nerbonne JM. Functional knockout of the transient outward current, long-QT syndrome, and cardiac remodeling in mice expressing a dominant-negative Kv4 α subunit. *Circ Res*. 1998; 83:560–567.
10. Wang L, Feng ZP, Kondo CS, Sheldon RS, Duff HJ. Developmental changes in the delayed rectifier K⁺ channels in mouse heart. *Circ Res*. 1996;79:79–85.
11. Xu H, Barry DM, Li H, Brunet S, Guo W, Nerbonne JM. Attenuation of the slow component of delayed rectification, action potential prolongation, and triggered activity in mice expressing a dominant-negative Kv2 α subunit. *Circ Res*. 1999;85:623–633.
12. Bou-Abboud E, Li H, Nerbonne JM. Molecular diversity of the repolarizing voltage-gated K⁺ currents in mouse atrial cells. *J Physiol*. 2000; 529(pt 2):345–358.
13. Rentschler S, Vaidya DM, Tamaddon HS, Degenhardt K, Sassoon D, Morley GE, Jalife J, Fishman GI. Visualization and functional characterization of the developing murine cardiac conduction system. *Development*. 2001;128:1785–1792.
14. Lev M, Thaemert JC. The conduction system of the mouse heart. *Acta Anat (Basel)*. 1973;85:342–352.
15. Myerburg RJ, Stewart JW, Hoffman BF. Electrophysiological properties of the canine peripheral A-V conducting system. *Circ Res*. 1970;26: 361–378.
16. Irisawa H, Brown HF, Giles W. Cardiac pacemaking in the sinoatrial node. *Physiol Rev*. 1993;73:197–227.
17. Anumonwo J, Jalife J. Cellular and subcellular mechanisms of pacemaker activity and synchronization in the heart. In: Zipes DP, Jalife J, eds. *Cardiac Electrophysiology: From Cell to Bedside*. St. Louis, Mo: WB Saunders Co; 1995:151–164.
18. DiFrancesco D. Pacemaker mechanisms in cardiac tissue. *Annu Rev Physiol*. 1993;55:455–472.
19. Verheule S, van Batenburg CA, Coenjaerts FE, Kirchhoff S, Willecke K, Jongsma HJ. Cardiac conduction abnormalities in mice lacking the gap junction protein connexin40. *J Cardiovasc Electrophysiol*. 1999;10: 1380–1389.
20. Bevilacqua LM, Simon AM, Maguire CT, Gehrmann J, Wakimoto H, Paul DL, Berul CI. A targeted disruption in connexin40 leads to distinct atrioventricular conduction defects. *J Interv Card Electrophysiol*. 2000; 4:459–467.
21. Weis SM, Emery JL, Becker KD, McBride DJ, Omens JH, McCulloch AD. Myocardial mechanics and collagen structure in the osteogenesis imperfecta murine (oim). *Circ Res*. 2000;87:663–669.
22. Morley GE, Vaidya D, Jalife J. Characterization of conduction in the ventricles of normal and heterozygous Cx43 knockout mice using optical mapping. *J Cardiovasc Electrophysiol*. 2000;11:375–377.
23. Carbonell LM. Esterases of the conductive system of the heart. *Histochem Cytochem*. 1955;4:87–97.
24. Escande D, Loisance D, Planche C, Coraboeuf E. Age-related changes of action potential plateau shape in isolated human atrial fibers. *Am J Physiol*. 1985;249:H843–H850.
25. Kilborn MJ, Fedida D. A study of the developmental changes in outward currents of rat ventricular myocytes. *J Physiol*. 1990;430:37–60.
26. Antzelevitch C, Sicouri S, Litovsky SH, Lukas A, Krishnan SC, Di Diego JM, Gintant GA, Liu DW. Heterogeneity within the ventricular wall: electrophysiology and pharmacology of epicardial, endocardial, and M cells. *Circ Res*. 1991;69:1427–1449.
27. Fedida D, Giles WR. Regional variations in action potentials and transient outward current in myocytes isolated from rabbit left ventricle. *J Physiol*. 1991;442:191–209.

28. Clark RB, Bouchard RA, Salinas-Stefanon E, Sanchez-Chapula J, Giles WR. Heterogeneity of action potential waveforms and potassium currents in rat ventricle. *Cardiovasc Res*. 1993;27:1795–1799.

29. Nabauer M, Beuckelmann DJ, Uberfuhr P, Steinbeck G. Regional differences in current density and rate-dependent properties of the transient outward current in subepicardial and subendocardial myocytes of human left ventricle. *Circulation*. 1996;93:168–177.

30. Guo W, Xu H, London B, Nerbonne JM. Molecular basis of transient outward K$^+$ current diversity in mouse ventricular myocytes. *J Physiol*. 1999;521(pt 3):587–599.

31. Baker LC, London B, Choi BR, Koren G, Salama G. Enhanced dispersion of repolarization and refractoriness in transgenic mouse hearts promotes reentrant ventricular tachycardias. *Circ Res*. 2000;86:396–407.

32. Callewaert G, Carmeliet E, Vereecke J. Single cardiac Purkinje cells: general electrophysiology and voltage-clamp analysis of the pace-maker current. *J Physiol*. 1984;349:643–661.

33. Kirchhoff S, Nelles E, Hagendorff A, Kruger O, Traub O, Willecke K. Reduced cardiac conduction velocity and predisposition to arrhythmias in connexin40-deficient mice. *Curr Biol*. 1998;8:299–302.

34. Simon AM, Goodenough DA, Paul DL. Mice lacking connexin40 have cardiac conduction abnormalities characteristic of atrioventricular block and bundle branch block. *Curr Biol*. 1998;8:295–298.

35. Xu H, Guo W, Nerbonne JM. Four kinetically distinct depolarization-activated K$^+$ currents in adult mouse ventricular myocytes. *J Gen Physiol*. 1999;113:661–678.

36. Priori SG, Mantica M, Napolitano C, Schwartz PJ. Early afterdepolarizations induced in vivo by reperfusion of ischemic myocardium: a possible mechanism for reperfusion arrhythmias. *Circulation*. 1990;81:1911–1920.

37. Rubart M, Pressler ML, Pride HP, Zipes DP. Electrophysiological mechanisms in a canine model of erythromycin-associated long QT syndrome. *Circulation*. 1993;88:1832–1844.

38. Zeng J, Rudy Y. Early afterdepolarizations in cardiac myocytes: mechanism and rate dependence. *Biophys J*. 1995;68:949–964.

39. Damiano BP, Rosen MR. Effects of pacing on triggered activity induced by early after depolarizations. *Lab Invest*. 1984;69:1013–1025.

40. Guo W, Li H, London B, Nerbonne JM. Functional consequences of elimination of $I_{to,f}$ and $I_{to,s}$: early afterdepolarizations, atrioventricular block, and ventricular arrhythmias in mice lacking Kv1.4 and expressing a dominant-negative Kv4 α subunit. *Circ Res*. 2000;87:73–79.